Separation and Purification Technology 326 (2023) 124780

Contents lists available at ScienceDirect

Separation and Purification Technology

journal homepage: www.elsevier.com/locate/seppur

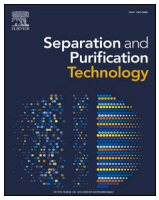

Recovery of nickel from spent multilayer ceramic capacitors: A novel and sustainable route based on sequential hydrometallurgical and photocatalytic stages

Marica Muscetta [a,*], Roberto Andreozzi [a], Laura Clarizia [a], Raffaele Marotta [a], Giovanni Palmisano [b], Grazia Policastro [c], Marco Race [d], Ahmed Yusuf [b], Ilaria Di Somma [e,*]

[a] Department of Chemical, Materials and Production Engineering (DICMaPI), University of Naples Federico II, Piazzale V. Tecchio 80, 80125 Naples, Italy
[b] Department of Chemical and Petroleum Engineering, Research and Innovation Center on CO2 and Hydrogen (RICH), Khalifa University of Science and Technology, Abu Dhabi, United Arab Emirates
[c] Telematic University Pegaso, 80100 Napoli, Italy
[d] Department of Civil and Mechanical Engineering, University of Cassino and Southern Lazio, Via Di Biasio 43, 03043 Cassino, Italy
[e] Institute of Sciences and Technologies for Sustainable Energy and Mobility (STEMS) of the National Research Council (CNR), Italy

ARTICLE INFO

Keywords:
Green leaching
Spent capacitors
Nickel recovery
Nickel dissolution
Photodeposition

ABSTRACT

The depletion of primary metal sources and the extensive use of nickel necessitate its extraction from secondary resources. In this study, we employed a chloride-based solution containing cupric ions ($NaCl/CuCl_2$) to enable a straightforward recovery process for nickel from Ni-containing waste materials. Prior to application in real systems, we evaluated different operating conditions using metallic nickel particles, including chloride and cupric ion concentrations, system temperature, and pH. Optimal efficiency was achieved at T = 60 °C, pH = 5.0, $[Cu(II)]_0 = 5.0 \times 10^{-3}$ M, and $[Cl]_0 = 6.0$ M, resulting in complete dissolution of metallic Ni (58 ppm) within 180 min. This optimized leaching system was then applied to exhausted nickel-containing multilayer ceramic capacitors (MLCCs) matrixes, leading to 80% Ni recovery. FESEM-EDX and XRD analysis characterized both synthetic and real matrixes. Additionally, we proposed a viable route for selective metal recovery through precipitation and photodeposition on titanium dioxide. Complete copper photodeposition occurred after 150 min, while Ni precipitation as $Ni(OH)_2$ was achieved by adjusting the solution pH to 10. Experimental data from runs with the synthetic matrix were analyzed using a shrinking spherical particle model.

1. Introduction

The advancements in commercializing lithium-ion batteries and Nickel metal hydride batteries have led to a significant increase in demand for metals like nickel [1]. The estimated demand for nickel is expected to reach approximately 1 million t/y by 2030, driven by the production of electric vehicles [1–3]. However, worldwide nickel resources are in short supply, and nickel currently is sold for 17,000 $/t and its price still rising [4].

Nickel's widespread use in industrial processes, such as methanation, steam reforming, hydrotreating, hydrodesulfurization, and vegetable oil hydrogenation [5–8], is due to its low cost and high reactivity [5,9,10]. In various commercial catalysts, nickel content typically ranges from 10 to 25% wt. [11]. Moreover, in the electronics industry, nickel serves as a cost-effective alternative to more expensive precious metals like silver (Ag) and palladium (Pd) in multilayer ceramic capacitors (MLCCs) [12,13].

The increasing popularity of electric cars has resulted in a higher demand for MLCCs known for their durability, high electrical voltage tolerance, and reliability [14]. MLCCs typically consist of multiple layers of ceramic $BaTiO_3$, acting as a dielectric substance, with inner electrodes made of nickel (with nickel content ranging between 12 and 20 % wt.) [15]. These capacitors comprise more than 800 submicron-thin dielectric layers, where the thickness of the active layer affects the electric field across the dielectric [16,17]. Achieving higher volumetric efficiency of capacity requires increasing the number of dielectric layers and reducing their thickness to the submicron range [18]. Hong et al. [19] reported that the number of MLCCs on a single mobile phone

* Corresponding authors.
E-mail addresses: marica.muscetta@unina.it (M. Muscetta), ilaria.disomma@stems.cnr.it (I. Di Somma).

https://doi.org/10.1016/j.seppur.2023.124780
Received 15 June 2023; Received in revised form 27 July 2023; Accepted 8 August 2023
Available online 9 August 2023

increased from 100 to 1100 in 10 years (2008–2018), and these represent only about 5% of the total number of capacitors used in the various electronic equipment. The escalating demand for nickel and the depletion of primary metal resources have made it essential to explore nickel recovery from secondary sources. Currently, spent materials, such as e-waste containing MLCCs, represent a significant secondary source for nickel recovery [5,11,20–22]. As an example, the production of a large amount of e-waste containing MLCCs is an excellent secondary source for nickel recovery [12]. Generally, the most employed processes for the recovery of nickel are pyrometallurgy and hydrometallurgy. Hydrometallurgy involves leaching metals by using organic or inorganic acids or ammonia solutions [1,23–26]. For instance, some researchers [18] have developed a hydrometallurgical process to recover different metals (Li, Ni, Co, and Al) from spent lithium-ion batteries. They recorded the best leaching efficiency in HCl solution, due to the presence of chloride ions able to promote nickel dissolution.

Additionally, Lim et al. [6] conducted an evaluation of the influence of an ultrasonic bath on the sulfuric acid-based leaching of spent silica-supported nickel hydrogenation catalysts. The study reported a remarkable nickel recovery of 99% in just 2 h at a leaching temperature of 60 °C and a nitric acid concentration of 12.5 vol%.

Nickel and copper recovery from jarosite was achieved through a combination of thermal and hydrometallurgical treatments with high efficiency in metal recovery when leaching was carried out in deionized water after the thermal treatment at 650 °C[4]. In a different study, Prabaharan et al. [27] proposed the selective recovery of metals from MLCCs through the combination of three different leaching steps: *(i)* base metals (Ba, Ti, Sn, Cu and Ni) were leached through the utilization of 10% (v/v) of HCl, *(ii)* the dissolution of Au and Pd was performed in the presence of aqua regia, and *(iii)* nitric acid was used to dissolve Ag from the residue.

Hydrometallurgical recovery of metals has been the go-to technique. Nevertheless, it is stymied by the disadvantageous use of strongly acidic conditions and high temperatures. Therefore, researchers have been investigating the development of alternative environmentally benign routes. An example was proposed by Yazici et al. [28], which obtained 98% of extractions for copper, nickel and iron within 120 min from waste-printed circuit boards in the presence of HCl, $CuCl_2$ and NaCl. Similarly, in a recent study [29], the optimal amounts of chloride and cupric ions were evaluated for the dissolution of metallic palladium nanoparticles in the presence of NaCl and $CuCl_2$ under moderately acidic conditions. Herein, an analogous process was employed for the recovery of nickel from the real exhausted nickel-containing MLCCs, as an alternative green methodology to the common techniques. Moreover, a novel combination of the leaching process with photocatalysis was proposed to effectively obtain the separation of the main leached metals (i.e., Cu and Ni). Photocatalytic technology, commonly employed for metal-based materials' preparation [30–32], proves to be promising for metal recovery as well [33]. This combined approach offers a viable and intriguing pathway to recover nickel selectively and easily from spent materials, utilizing non-toxic chemicals, lower temperatures, mildly acidic conditions, and the possibility of harnessing solar energy for efficient metal separation with high purity.

Before applying this technique to real spent materials, various operating parameters and conditions were explored using pure metallic nickel to establish optimal leaching process conditions. The study investigated the effect of the temperature and pH of the suspension and the concentration of the oxidizing agent on the leaching process. Additionally, a mathematical model of the system was developed and validated with experimental data. Once the synthetic system was thoroughly investigated, nickel-containing exhausted MLCCs were treated under optimized conditions, by combining the leaching process with the photocatalytic technique.

2. Materials and methods

2.1. Process description

In Fig. 1, the block diagram of the process for nickel recovery from exhausted Ni-MLCCs is summarized. The pre-processing step consists of dismantling and crushing the real e-waste (i.e., MLCCs) by using a pestle and mortar to obtain a fine powder. Then, a solution containing NaCl/$CuCl_2$ (Unit (2): $[NaCl]_0 = 6.0$ M; $[CuCl_2]_0 = 5.0 \bullet 10^{-3}$ M; T = 60 °C; pH = 5.0) was used to oxidize Ni(0) to Ni(II), thus producing two different phases: a liquid phase mainly made of Ni(II) and the leaching solution, and a solid phase containing the metals which did not dissolve. In a photocatalytic reactor, TiO_2 nanoparticles (500 ppm) were used to treat the solution produced by the leaching unit (2). The photodeposition process takes place in the presence of a hole organic scavenger (bioethanol, 2.5 M), under UV-A/visible light radiation and nitrogen flow (0.3 $L \bullet min^{-1}$). The obtained liquid phase product contained the ionic species (Ni^{2+}, Na^+ and Cl^-) which were not photodeposited. Nickel could be consequently easily recovered through an alkalinization of the solution (pH ≈ 10.0), thus obtaining a $Ni(OH)_2$, a promising electrocatalyst for hydrogen evolution [34,35]. The solid phase made of a Cu/TiO_2 material can be treated with an air flux (0.3 $L \bullet min^{-1}$) able to oxidize the copper species, thus obtaining the separation of the metal (i.e., copper in the form of Cu(II)) from the catalyst (i.e., TiO_2).

2.2. Materials

Copper chloride (CuCl2 powder-99% w/w), sodium chloride (NaCl ≥ 99% w/w) and ethanol (absolute) were bought from Aldrich Chemistry. Nickel (powder, <1 μm, ≥99.9 % trace metals basis) was received from Carlo Erba. Bioethanol was purchased by AnalaR BDH supplied potassium hydroxide pellets and perchloric acid (70% v/v). Doubly glass–distilled water was used throughout this investigation. Waste MLCCs were obtained by manual disassembly of different electric and electronic components (waste printed circuit boards, WPCBs).

2.3. Experimental procedure

2.3.1. Leaching experiments

In the leaching experiments, an annular glass batch reactor with a thermostatic jacket set to a specific temperature, nickel leaching runs were conducted (This setup is depicted in Fig. S-1 (a)). During the leaching runs (Unit (2) of Fig. 1), a fixed amount of metallic nickel (11.6 mg) was used and immersed in an aqueous solution (V = 0.20 L) with controlled pH (ranging from 2.5 to 7.0), temperature (ranging from 20 to 60 °C), and concentrations of $CuCl_2$ (ranging from 0 to $5.0 \bullet 10^{-3}$ M) and sodium chloride (ranging from 0 to 6.0 M). To maintain particles suspended and minimize the impact of liquid–solid mass transfer limitations on the kinetic process, the solid–liquid suspension was continually stirred at 500 rpm.

In evaluating the nickel oxidation, multiple samples were collected at various time intervals during the leaching runs. For experiments involving real spent material, we first dismantled and shredded the material in a mortar (Unit (1) of Fig. 1). The resulting powder (60 mg) was then introduced into an aqueous solution with fixed pH (5.0) and temperature (60 °C), along with a fixed concentration of $CuCl_2$ (the copper chloride concentration was fixed at 5 times the expected nickel concentration) and sodium chloride (6.0 M) (Unit (2) of Fig. 1). This suspension was continuously stirred at 500 rpm, and we collected multiple samples at various time points during the experimental runs to assess the nickel dissolution kinetics. After the leaching process, the solid was collected, dried, and submitted to material characterization. All the experiments were repeated three times to ensure reliable and consistent results.

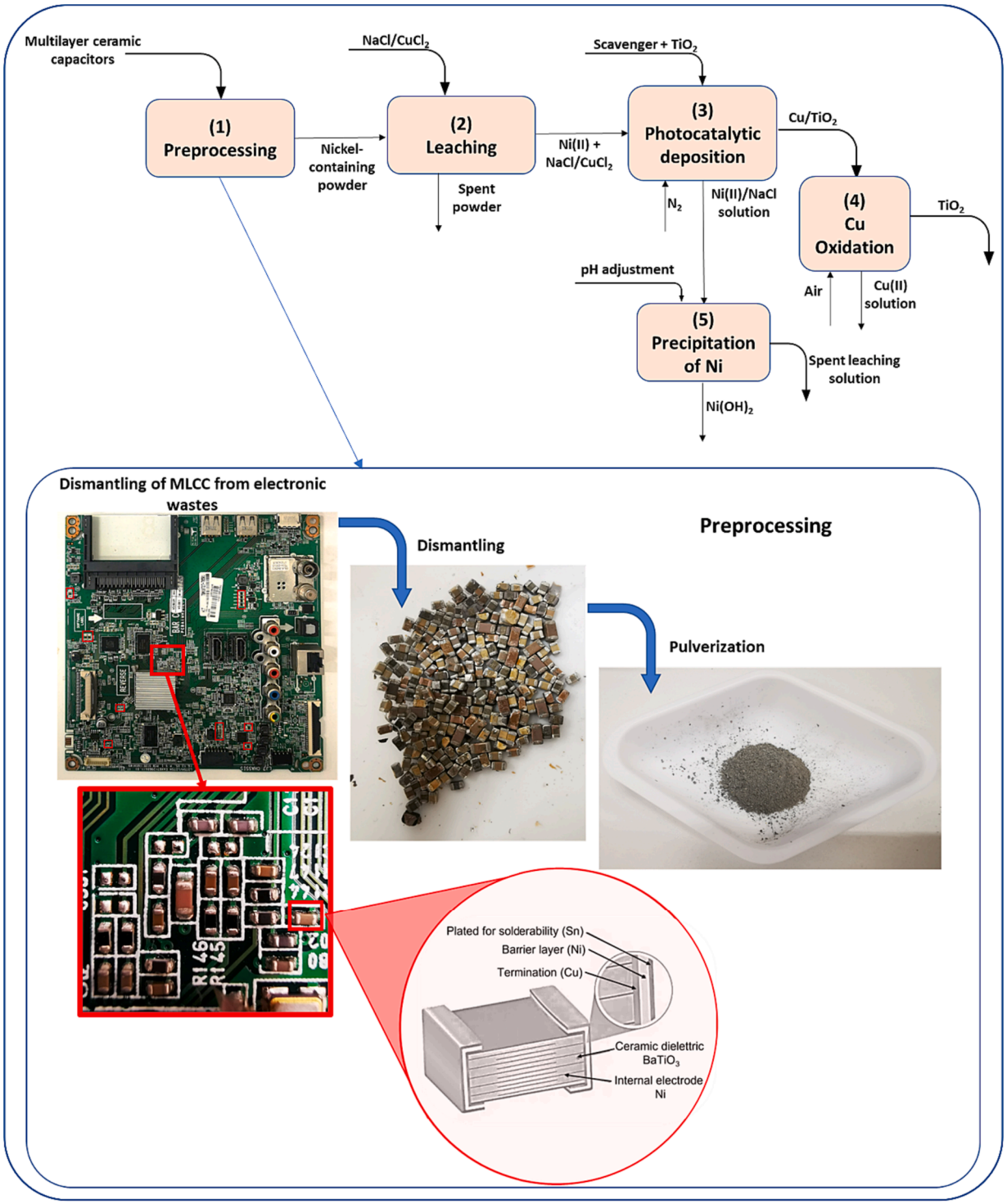

Fig. 1. Illustration of the Key Stages in the Proposed Process. Inset: Key Stages in the Pre-Processing Unit.

2.3.2. *Photocatalytic experiments*

The photocatalytic runs were conducted in an annular glass batch reactor, featuring a high-pressure mercury vapour lamp (125 W power input by Helios Italquartz) situated in a quartz sleeve, as reported elsewhere (see Fig. S-1 (b) for the experimental set-up) [33]. In this case, a bioethanol solution (2.5 M) was mixed with the solution derived from Unit (2). An N_2 stream (0.3 L•min^{-1}) was bubbled 40 min before the experimental run, in order to avoid the reaction between oxygen and photogenerated electrons. Subsequently, a specific amount of TiO_2 (150 mg) was then transferred into the solution. Nitrogen was continually pumped into the reactor throughout the photocatalytic run. After the reaction, the solid material was recovered as mentioned elsewhere [36].

2.3.3. *Recovery of $Ni(OH)_2$ and Cu(II)*

After the photodeposition process, the recovered solid material (Cu/TiO_2) was suspended in a doubly distilled aqueous solution. In this case, an air stream (flow rate of 0.3 L•min^{-1}) for 120 min was employed to oxidize the copper species deposited on the surface of the photocatalyst. The suspension was thus filtered to effectively obtain a solution mainly composed of Cu(II). Moreover, the liquid phase obtained after Unit (3)

was treated by modifying the pH of the solution up to a value of 10, resulting in the precipitation of the Ni(II). The precipitate was then collected and dried at 120 °C for 2 h, thus obtaining the nickel-based desired product.

2.4. Material characterization

The metal content was evaluated in the tested MLCCs. Inductively coupled plasma-mass spectroscopy (ICP-MS) was performed with (Perkin ElmerNexION 2000) to determine the concentration of metals in the pre- and post-leaching materials. The ICP-MS program employed is as follows: a blank flushing time of 45 s between each run, 35 s for sample flushing then, 15 s read delay, 40 s analysis time, nebulizer gas flow of 0.80 L/min and the dual detection mode was used. Prior to the ICP-MS analysis, 10 mg of the materials were first digested using a CEM Mars 6 microwave digestion system at a temperature of 210 °C for 30 mins in a 10 mL mixture of concentrated HNO_3, HCl, and H_2SO_4 with a volumetric ratio of 1:3:12, respectively. After cooling, the digestate was analysed using the ICP-MS. In some cases, atomic Absorption Spectrometry (AAS) with a Varian Model 55B SpectrAA (F-AAS) was employed to measure metal concentration [37]. A field-emission scanning electron microscope (FESEM; Quanta 3D, FIB) was utilized to visualize and analyse the microstructure morphology of all materials. The samples were fixed on metallic SEM stubs with double-sided carbon tape. The elemental mapping of each sample was performed with the energy-dispersive X-ray (EDX) probe equipped with the FESEM. The dimension and shape of the MLCCs samples were evaluated by means of an optical microscope (ZEISS AXIOSCOPE 2 PLUS) equipped with a digital camera (Camera P12 Pro, color, CMOS, 1/1.7″, 12MP USB 3.0) in bright field transmission mode at 3x magnification. A PANanalytical diffractometer, with a nickel filter and Cu K radiation, was used to record the materials' X-ray diffraction (XRD) patterns.

3. Results and discussion

3.1. Material characterization

In Fig. 2, the SEM micrographs of the commercial nickel powder are reported. In Fig. 2 (a) the particles appear round and porous, with a relatively narrow size distribution between 3 μm and 10 μm (see inset in Fig. 2 (a)). Fig. 2 (b) and (c) allow a closer look at the morphology of the particle surface, which is approximately spherical with hierarchical flower-like morphology.

As concerns the real matrix, after the pulverization, MLCC powders underwent a thorough characterization able to assess the following physicochemical aspects: *(i)* metal composition, *(ii)* granulometric distribution, and *(iii)* morphology of the sample. The metal composition (% wt.) is reported in Table 1. As indicated, nickel represents nearly 20% of the total amount of spent material. The most abundant species are barium and titanium, which represent the main components of the dielectric material (Barium titanate, $BaTiO_3$). The results reported in Table 1 agree with those reported in the literature [12,27,38].

The particle size distribution was evaluated to better understand the leaching process in the real case. Fig. 3 (a) and (b) show the SEM micrographs of the Ni-based MLCC. As clearly highlighted in Fig. 3 (c), a wide size distribution is observed. About 33% wt. of the pulverized matrix is made of particles with a size smaller than 70 μm, whereas 28% wt. is characterized by larger particles (>300 μm). Based on the wide heterogeneity of the solid sample, the metal composition for each fraction can be extremely different from Table 1. For this reason, the metal composition was evaluated also for each fraction, as reported in Table 2. A wide range of the metal composition is observed in Table 2 by varying the granulometric fraction. The highest content in Ba and Ti (corresponding to the highest content in barium titanate $BaTiO_3$) can be observed in Fraction 2. On the other hand, the highest content in Ni was observed in Fraction 4, despite the Ni content being higher than 19% wt. for all the fractions. A higher content of Cu was observed in the fractions with larger particle sizes, probably due to the presence of this metal in

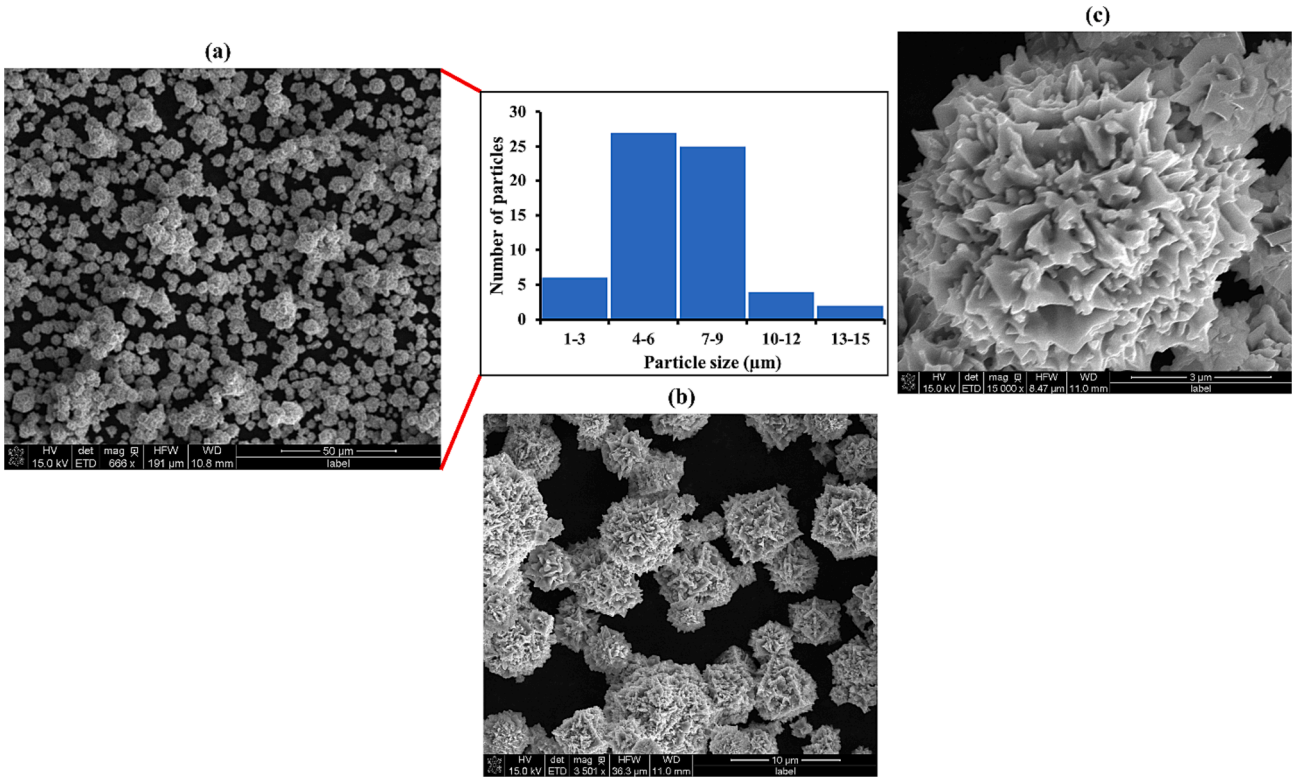

Fig. 2. SEM images of the commercial nickel powder (a) showing estimated particle size distribution (b) at 3501× magnification (c) at 15,000x magnification.

Table 1
Composition of Ni-MLCCs (wt. %) determined by ICP-MS.

Element	Ba	Ca	Cu	Ni	Sn	Ti	Other*	Acid Insoluble**
%wt.	41.81	1.55	4.03	20.4	3.36	18.65	2.73	7.47

*Other corresponds to the sum of all metals present in percentage with a composition lower than 1%wt. (i.e., Ag, Zn, Bi, Pt).
**Acid Insoluble represents the fraction of MLCC insoluble in acid.

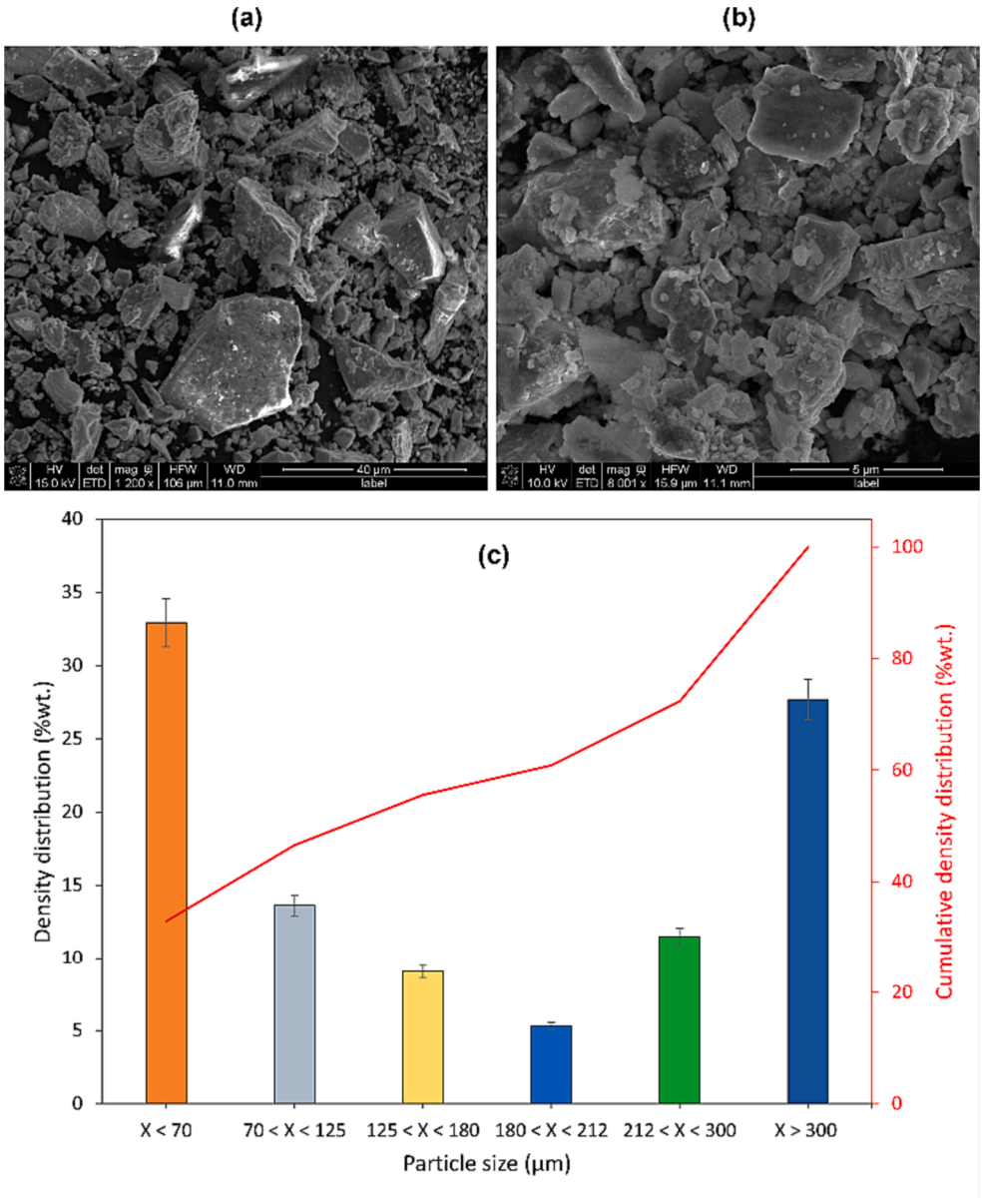

Fig. 3. (a, b) SEM images of the pulverized Ni - MLCC. (c) Particle size distribution of the spent Ni-MLCC. Red line: cumulative density size distribution. (For interpretation of the references to color in this figure legend, the reader is referred to the web version of this article.)

the plates and terminations of the capacitor, which are more difficult to be shredded. Fig. S-2 reports optical microscope images of the solid particles at different granulometric fractions obtained after the pulverization of the real matrixes (Ni-MLCC). As indicated in Fig. S-2, a wide irregular shape distribution was observed for all the particle sizes. After the leaching process, the shape of the samples resulted unmodified (data not shown). Fig. S-3 reports the XRD patterns of the Ni-MLCC at different granulometric fractions. The peaks in Fig. S-3 reveal the presence of $BaTiO_3$, Ni, and Cu in the sample for all the granulometric fractions considered, as confirmed by the metal composition analysis.

3.2. *Leaching optimization. Pure nickel-containing powder*

3.2.1. *Effect of different parameters on the leaching process*

Based on the current literature survey, it is evident that leaching processes often take place under harsh acidic conditions, leading to significant environmental concerns. However, some studies [29], have explored the possibility of using milder conditions, particularly for palladium and silver dissolution. In this context, we present a novel and effective approach for nickel dissolution.

Before implementing the leaching process on real matrixes, we

Table 2
Composition of Ni-MLCCs (wt. %) for each fraction determined by ICP-MS. X = Particle dimension.

	Element	Ba	Ca	Cu	Ni	Sn	Ti	Other	Acid insoluble
1	Fraction X < 70 μm	44.55	1.53	1.17	17.52	3.23	17.41	2.66	11.94
2	70 μm < X < 125 μm	44.57	2.34	1.77	20.53	2.98	21.60	2.15	4.07
3	125 μm < X < 180 μm	40.53	2.15	3.81	19.10	2.52	19.01	3.15	9.74
4	180 μm < X < 212 μm	34.76	2.48	6.47	26.08	5.81	16.84	4.32	3.23
5	212 μm < X < 300 μm	41.46	2.39	5.82	19.86	3.36	18.57	3.32	5.21
6	X > 300 μm	39.11	0.47	7.41	23.31	3.49	18.95	2.41	4.85

*Other corresponds to the sum of all metals present in percentage with a composition lower than 1%wt. (i.e., Ag, Zn, Bi, Pt).
**Acid Insoluble represents the fraction of MLCC insoluble in acid.

thoroughly investigated various operating parameters and conditions using pure metallic nickel to ensure optimal process efficiency and feasibility. Initially, we focused on evaluating the effect of pH on metal dissolution. Fig. 4 (a) reports the results obtained from various runs conducted in the presence of $CuCl_2$/NaCl solutions with different pH values. As clearly indicated by the trendlines in Fig. 4, the dissolved nickel amount increases as the pH of the suspension decrease from 7.0 to 5.0. Interestingly, no nickel dissolution occurs at neutral pH, possibly due to the precipitation of copper species as $Cu(OH)_2$, which prevents the oxidation of nickel, as indicated by the equilibrium in the reaction (1):

$$\frac{1}{2}Ni^0 + Cu^{2+} + 3Cl^- \leftrightarrow \frac{1}{2}NiCl^+ + \frac{1}{2}CuCl_2^- + \frac{1}{2}CuCl_3^{2-} \quad (1)$$

On the contrary, a similar behaviour was observed at pH 2.5 and 5.0, with a total dissolution of nickel after 30 min. For this reason, the system's pH was fixed at 5.0, representing the optimal pH that can be adopted to obtain an effective nickel recovery.

To determine the effect of cupric ions and chlorides on nickel dissolution, multiple tests were conducted by varying cupric ion and chloride concentrations. Fig. 4 (b) shows the fraction of dissolved nickel as a function of time. No nickel dissolution was observed when sodium chloride is absent. On the other hand, the nickel dissolution efficiency (controlled by the reaction (1)), increases by increasing the chloride amount due to the generation in the solution of chloro-complexes, with cupric species, which thus remain in solution for higher pH values [29,39]. Indeed, nickel dissolution is favourable in all cases, as it is clear considering the following half-reactions and their potentials (which result different from the values obtained in the absence of chloride ions [40]):

$$Ni^0 + Cl^- \leftrightarrow 2e^- + NiCl^+ \qquad E^0_{Ni} = 0.243V \quad (2)$$

$$Cu^{2+} + 2Cl^- + e^- \leftrightarrow CuCl_2^- \qquad E^0_{Cu1} = 0.470V \quad (3)$$

$$Cu^{2+} + 3Cl^- + e^- \leftrightarrow CuCl_3^{2-} \qquad E^0_{Cu2} = 0.433V \quad (4)$$

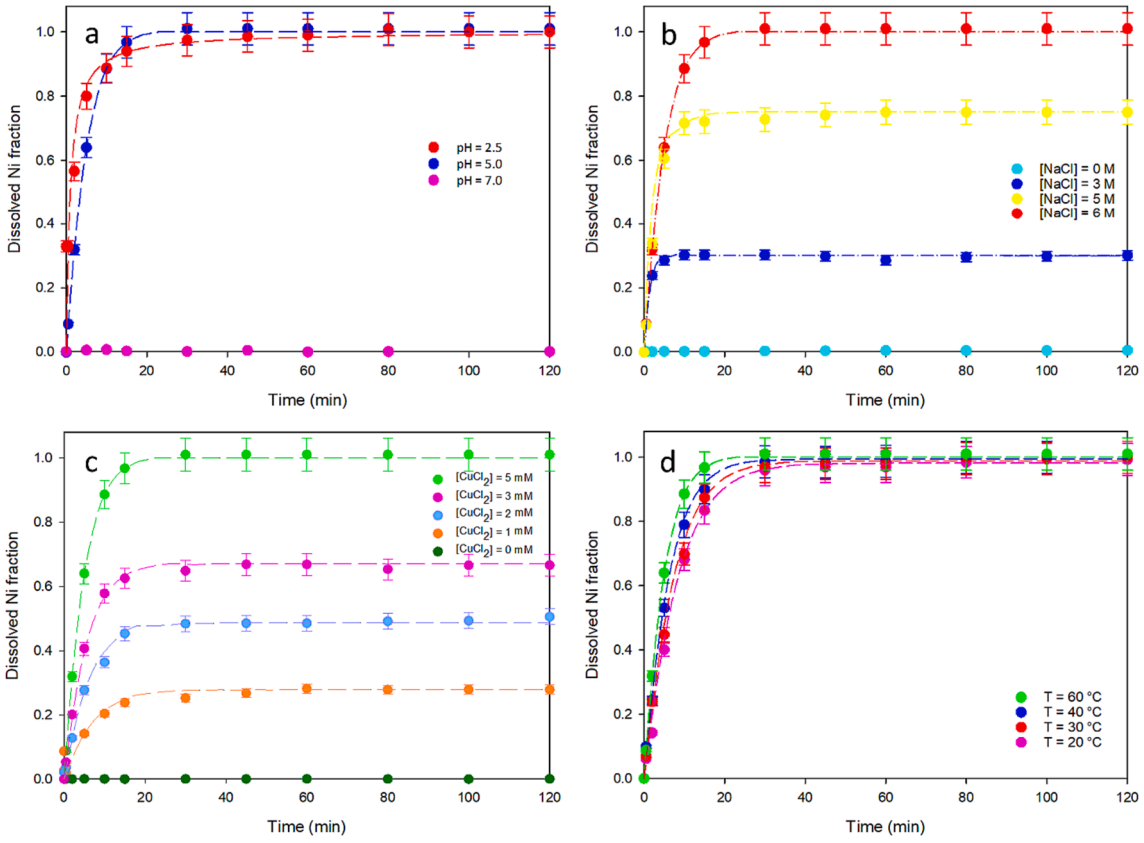

Fig. 4. Dissolved nickel fraction against time at different operating conditions (model predictions = continuous lines, experimental data = symbols). (a) pH effect, experimental conditions: $[NaCl]_0 = 6.0$ M; $C_{Ni} = 58$ ppm; $[Cu(II)]_0 = 5.0 \bullet 10^{-3}$M; V = 200 mL; T = 60 °C. (b) Chloride effect, experimental conditions: pH = 5.0; $C_{Ni} = 58$ ppm; $[Cu(II)]_0 = 5.0 \bullet 10^{-3}$M; V = 200 mL; T = 60 °C. (c) Cu(II) effect, experimental conditions: pH = 5.0; $[NaCl]_0 = 6.0$ M; $C_{Ni} = 58$ ppm; V = 200 mL; T = 60 °C. (d) Temperature effect, experimental conditions: pH = 5.0; $[NaCl]_0 = 6.0$ M; $C_{Ni} = 58$ ppm; V = 200 mL; $[Cu(II)]_o = 5.0 \bullet 10^{-3}$M.

Additionally, several experiments carried out at various cupric ion concentrations (See Fig. 4 (c)) revealed that improving the amount of the oxidizing agent (cupric ion) improved nickel dissolution. When the stoichiometric value of cupric ion was used ([Cu(II)]/[Ni(0)] = 2), about 50% nickel was oxidized. Otherwise, a total dissolution was obtained when the ratio between cupric ions and nickel concentration [Cu(II)]/[Ni(0)] in the system was fixed at 5. Based on the previous results, the chloride concentration was fixed to 6.0 M and the [Cu(II)]/[Ni(0)] was set at 5 to optimize the process.

Finally, Fig. 4 (d) reports the results of several dissolution experiments conducted at varying the operating temperature for a fixed number of leaching agents. Temperature affected the oxidation rate, even though the metal dissolved completely in all the experiments. In fact, the presented data reveal a good reactivity even at room temperature (i.e., 20 °C) and the dissolution of nickel within 2 h of reaction.

3.3. Mathematical modelling

The leaching process on pure nickel particles was mathematically described using the "shrinking spherical particles model with no ash formation" [41]. Based on the characterization tests performed on the synthetic matrix (i.e., commercial nickel powder), the shape of the nickel particles was approximately spherical. Considering the leaching reaction at the nickel/solution interface, the volume of the spherical particle progressively decreases, proceeding through *(i)* diffusion of the reagents (Cu(II)) and chloride ions) to the particle surface through the liquid film, *(ii)* superficial reaction, and *(iii)* diffusion of the products from surface of the particle to the liquid bulk. Fig. 5 reports the schematic of the mechanism for nickel dissolution.

Considering the speciation of chloride ions with copper and nickel, Reactions (5) and (6) can be considered for the nickel oxidation:

$$\frac{1}{2}Ni^0 + Cu^{2+} + \frac{5}{2}Cl^- \rightarrow \frac{1}{2}NiCl^+ + CuCl_2^- \quad (5)$$

$$\frac{1}{2}Ni^0 + Cu^{2+} + \frac{7}{2}Cl^- \rightarrow \frac{1}{2}NiCl^+ + CuCl_3^{2-} \quad (6)$$

Based on the sum of Reactions (5) and (6), and dividing by 2, reaction (1) is obtained; its equilibrium equation can be expressed as follows:

$$K_{eq} = \frac{[NiCl^+]^{\frac{1}{2}}[CuCl_2^-]^{\frac{1}{2}}[CuCl_3^{2-}]^{\frac{1}{2}}}{[Cl^-]^3[Cu^{2+}]} \bullet \prod \gamma_i \quad (eq1)$$

with γ_i being the activity coefficient of the species i involved in the equilibrium eq_1.

If the process proceeds under diffusive control, the nickel mass balance can be expressed by the following equation (eq_2):

$$-\frac{1}{4\pi R_{Ni}^2}\frac{dN_{Ni^0}}{dt} = -\frac{1/2}{4\pi R_{Ni}^2}\frac{dN_{Cu^{2+}}}{dt} = \frac{1}{2}k_L([Cu^{2+}] - [Cu^{2+}]_{eq}) \quad (eq2)$$

Where:

- R_{Ni} is the initial radius of the metallic nickel particles,
- N_{Ni^0} and $N_{Cu^{2+}}$ are moles of metallic nickel and cupric ions, respectively,
- k_L is the diffusion constant.

A detailed description of the model is reported in the Supplementary materials. The as-developed model may be employed to estimate X_{Ni} (zerovalent nickel conversion degree) when appropriated values for the parameters k_L, γ_i and K_{eq} are provided. The estimation of γ_i and K_{eq} was obtained through the procedure reported in a previous work [29]. In particular, K_{eq} (T = 25 °C) represents the square root of the product of the equilibrium constants obtained for the following reactions (see the Supplementary materials for the detailed calculations):

$$Ni^0 + 2Cu^{2+} \underset{\rightleftarrows}{K_1} Ni^{2+} + 2Cu^+ \quad (7)$$

$$Ni^{2+} + Cl^- \underset{\rightleftarrows}{K_2} NiCl^+ \quad (8)$$

$$Cu^+ + 2Cl^- \underset{\rightleftarrows}{K_3} CuCl_2^- \quad (9)$$

$$Cu^+ + 3Cl^- \underset{\rightleftarrows}{K_4} CuCl_3^{2-} \quad (10)$$

A nonlinear fitting of the developed model can be assessed to estimate the unknown k_L parameter [42]. An iterative optimization procedure that minimized the square of the differences between experimental and theoretical data was applied by simultaneously using different experimental results, at varying the following conditions: (*i*) temperature of the system; (*ii*) cupric ion concentration; (*iii*) chloride concentration. As clearly indicated in Fig. 6, k_L(i.e., the diffusive constant) is poorly affected by the temperature, ranging between 1.80×10^{-4} m•min^{-1} and 3.10×10^{-4} m•min^{-1} when the temperature increases from 293 K to 333 K, thus confirming that the process proceeds under diffusive control.

Fig. 4 (a–d) report the results of the model prediction obtained with the optimum values of the unknown parameters and the experimental data. A robust data accordance (i.e., a standard deviation of nearly 1.0%) was obtained, thus demonstrating the reliability of the as-developed model to simulate the behaviour of the nickel recovery process.

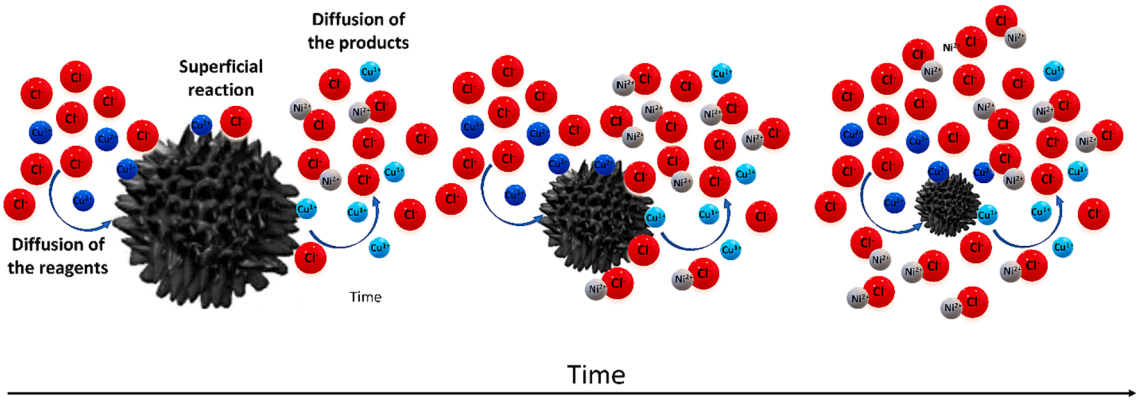

Fig. 5. Schematic representation of the nickel dissolution process.

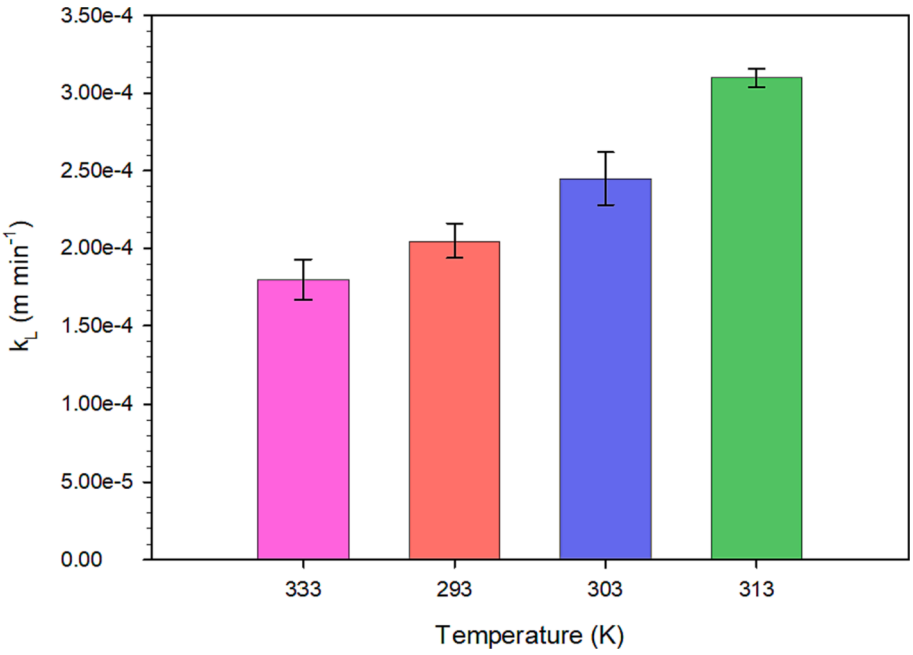

Fig. 6. Dependence of k_L against the temperature of the system.

3.4. Recovery of nickel from a real spent matrix: The case of exhausted MLCC capacitors

3.4.1. Leaching process for the dissolution of nickel from capacitors

Based on the results reported in the previous sections, further investigations have been performed on the recovery of nickel (and other metals if present) from real exhausted nickel containing MLCCs to assess the efficiency of the proposed procedure. When employing real matrices (see Fig. 1), the components located on different PCBs were firstly separated from the e-waste, then pulverized, and finally the nickel-containing parts were treated with the leaching solution by fixing the best conditions obtained in the previous sections (i.e., [Cu(II)]/[Ni(0)] = 5.0; $[NaCl]_0$ = 6.0 M; T = 60 °C; pH = 5.0).

The main results are reported in the Fig. 7 (a). With respect to the pure metal, a lower efficiency was recorded in the real case, recovering almost 80% Ni present in the powder. The different reactivity of the system in the real case can be ascribed to different phenomena. As indicated in the previous sections, the real matrix has a heterogeneous distribution of particle size, with a great number of particle diameters larger than 70 μm. Upon increasing the particles dimension, diffusive phenomena could negatively affect the efficiency of the process, as confirmed by the Fig. 7 (b), which reports the leaching efficiency for the different granulometric fractions. Moreover, with respect to pure metal particles, nickel is deposited either on the external powder surfaces with a different Ni percentage depending on particle shape and dimensions or among different layers in the pulverized Ni-MLCCs, thus reducing the efficiency of the leaching phenomenon. The inset in Fig. 1 reports the schematic representation of a typical Ni-MLCC. Despite the different metals observed in the real matrix (as reported in Tables 1 and 2), a negligible amount of the other metals was found in the spent leaching solution (See Table S-1 for the removal efficiencies of each metal). Only copper was oxidized along with nickel during the leaching process and represents one of the main components of the leaching solution. Hence, the obtained solution was successively treated to effectively separate nickel and copper (See the section presented below).

3.4.2. Photocatalytic and alkalization processes for nickel recovery from leached aqueous matrices

As reported in the process schematic shown in Fig. 1, nano-TiO_2 based photocatalytic process was carried out to selectively separate

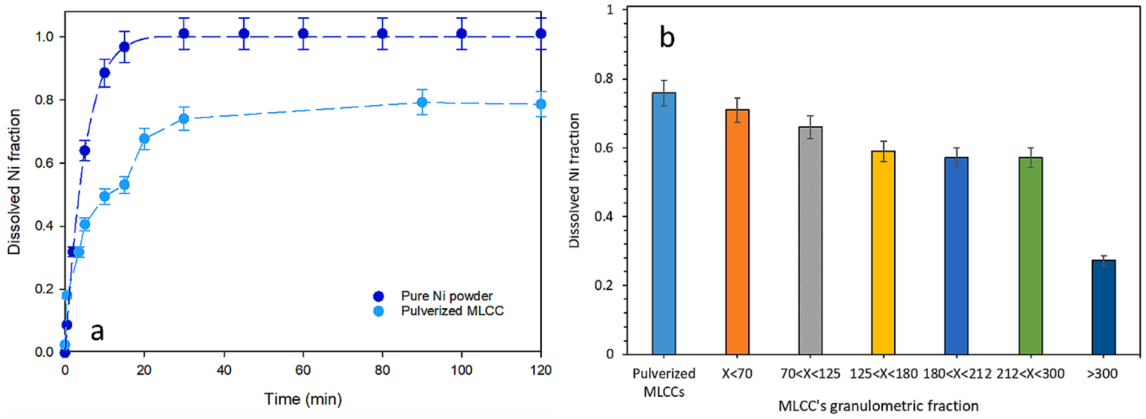

Fig. 7. (a) Dissolved nickel fraction against time from pure Ni powders (blue symbols) and pulverized MLCCs (light blue symbols). (b) Dissolved nickel fraction after 120 min from different MLCC's granulometric fractions. Experimental conditions: Pure Ni powder amount = 21 mg (MLCCs powder amount = 60 mg); $[NaCl]_0$ = 6.0 M; $[Cu(II)]_0 = 5.0 \bullet 10^{-3}$ M; V = 200 mL; T = 60 °C; pH ≈ 4.5.

copper from nickel after the leaching unit (Unit (2)) (see also Fig. 8 (a)). The complete copper photodeposition occurred after ca. 150 min. Conversely, no nickel deposition was observed likely due to the unsuitable redox potential, as reported in literature [43]. Once separated the solid phase from the solution, the obtained material was suspended in aqueous solution and treated with an air flux able to oxidize the copper species (see Fig. S-4). After 120 min of bubbling, almost 100% of the cupric ions were reoxidized, suggesting the effective separation of copper from the catalyst, as well the possibility to regenerate the photocatalyst on-site by infusing a stream of air into the suspension, as proposed by others [44].

The leaching solution coming from the unit (3) was then treated by adjusting the pH up to 10 and obtaining the complete nickel precipitation in the form of $Ni(OH)_2$ (See Fig. 8 (b)). As indicated in Fig. 9, all the diffraction peaks can be indexed are related to the hexagonal phase of β-$Ni(OH)_2$ (JCPDS, file No. 14-0117); the presence of impurities was not observed, indicating the effectiveness of the separation process.

3.4.3. *Efficiency of the whole proposed process*

Based on the previous results, we assessed the effective separation of Ni from spent Ni-MLCC by performing a mass balance of the metal (along with copper), on the entire process.

As reported in the Fig. 10, when a certain amount of Ni-MLCC material (in which 11.60 mg of Ni and 2.30 mg of Cu are present), was treated with the optimized leaching solution, 9.12 mg of Ni^{2+} were obtained. The Ni recovery efficiency in the leaching unit is 80%, as indicated in the Fig. 7 (a). As clearly shown, a large amount of cupric ions (65.62 mg) is present in the stream coming from the unit (2), which is treated through photodeposition on titanium dioxide, obtaining a high efficiency in terms of copper separation from the solution containing nickel. Through the oxidation of zero-valent copper to Cu(II) with air stream bubbling, copper was almost completely separated and recovered, with a very small amount of nickel present in this stream (0.09 mg). As concerns the liquid solution coming from the photodeposition unit, 8.98 mg were recovered through precipitation as $Ni(OH)_2$. In this case, small impurities of Cu (0.46 mg) present as $Cu(OH)_2$ were obtained, thus confirming the effective separation of the two metals.

4. Conclusion

A mildly acidic leaching technique has proven to be effective in dissolving metallic nickel, both from pure nickel powder and pulverized MLLC waste. Optimal operating conditions (i.e., [Cu(II)]/[Ni(0)] = 5.0; [NaCl] = 6.0 M; T = 60 °C; pH = 5.0) resulted in approximately 80% nickel dissolution from multilayer ceramic capacitors obtained from e-wastes. The leaching efficiency was influenced by particle size, where larger particles exhibited lower process efficiency. To selectively separate copper and nickel, we proposed photodeposition and precipitation

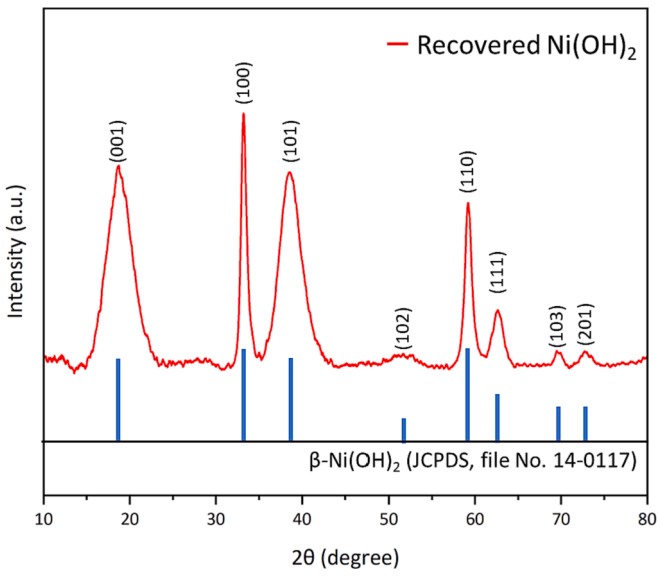

Fig. 9. XRD patterns of the solid recovered after the precipitation.

steps after oxidizing nickel. Starting from the spent Ni-MLCC powder, $Ni(OH)_2$ with high purity was obtained after precipitation. Moreover, the use of the subsequent oxidation of copper post-photodeposition unit leads to the effective recovery of this metal, which can be easily reused as a leaching agent.

In the case of pure nickel powder, the leaching process operated under diffusive control. A shrinking spherical particles model was used to successfully analyze the experimental data obtained during the runs. The diffusive constant k_L is poorly influenced by the temperature, thus confirming that the process proceeds under diffusive control.

This newly developed leaching method offers an intriguing sustainable technique for easily and selectively recovering nickel from spent materials, employing low temperatures, moderate acidic conditions, and non-toxic chemicals. The approach is particularly useful for recycling e-waste with a high nickel content and holds promise for other nickel-containing waste materials.

Looking ahead, we propose two outlooks to reduce the environmental impact of the process further: (i) reusing the leaching solution for subsequent leaching processes and (ii) recycling TiO_2 nanoparticles back to the photodeposition unit. These measures aim to enhance the overall environmental sustainability of the entire process.

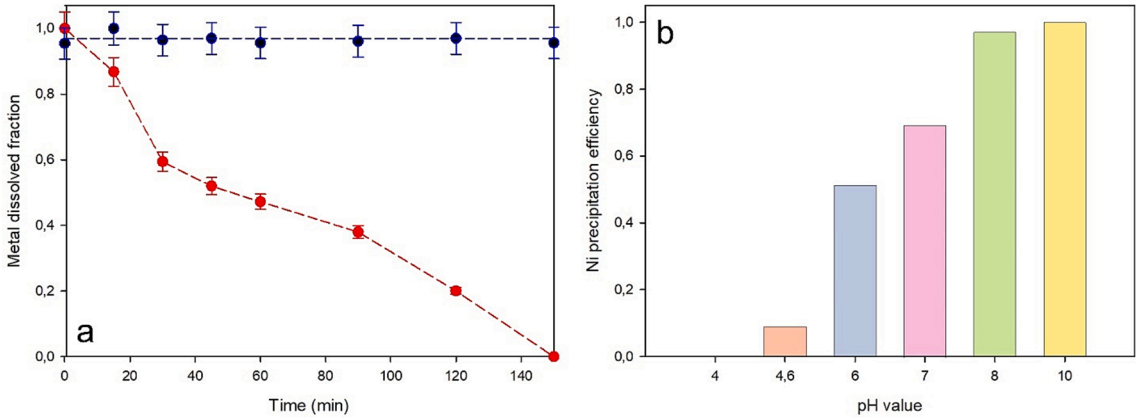

Fig. 8. (a) Dissolved metal fraction against time (red symbols) Cu(II); (blue symbols) Ni(II); (b) Nickel precipitation efficiency against pH values.

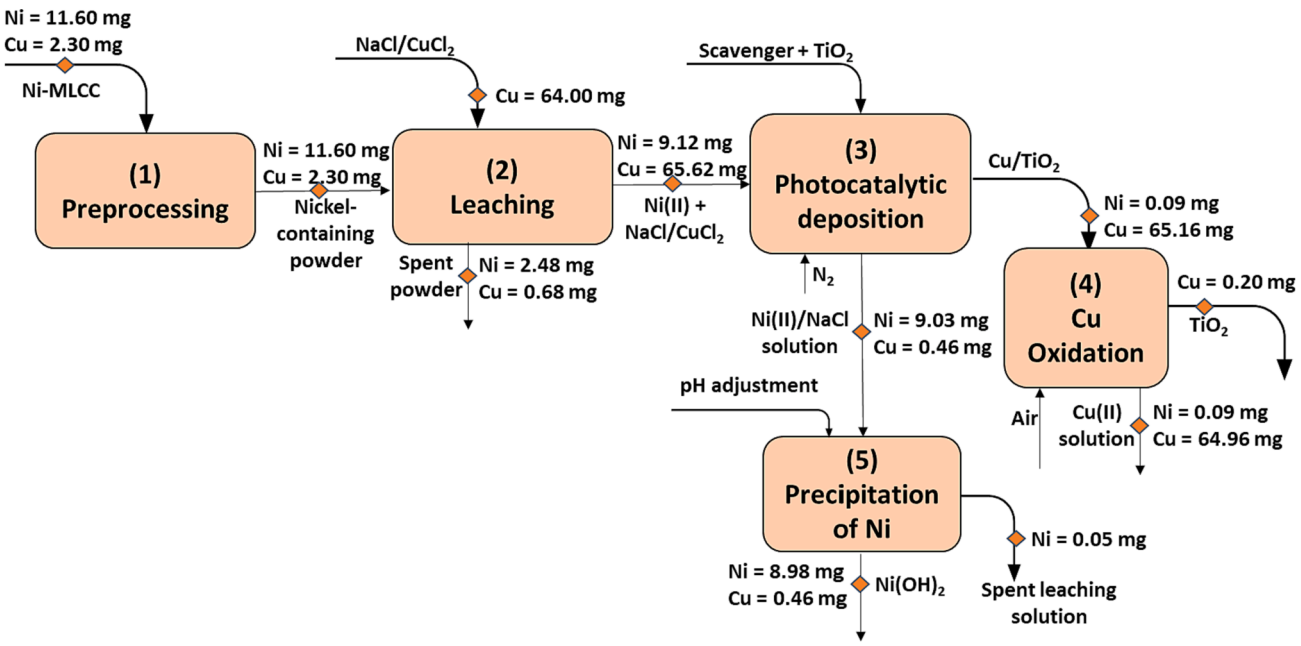

Fig. 10. Mass balance of Ni and Cu on the entire process. All the experiments were carried out in a reaction volume of 0.200 L.

CRediT authorship contribution statement

Marica Muscetta: Conceptualization, Investigation, Data curation, Writing – original draft, Writing – review & editing. **Roberto Andreozzi:** Conceptualization, Investigation, Writing – review & editing, Supervision. **Laura Clarizia:** Data curation, Writing – original draft, Investigation. **Raffaele Marotta:** Investigation, Writing – review & editing, Supervision. **Giovanni Palmisano:** Conceptualization, Writing – review & editing, Supervision. **Grazia Policastro:** Data curation, Investigation. **Marco Race:** Writing – original draft, Investigation, Data curation. **Ahmed Yusuf:** Investigation, Data curation, Writing – original draft, Writing – review & editing. **Ilaria Di Somma:** Data curation, Validation, Formal analysis.

Declaration of Competing Interest

The authors declare that they have no known competing financial interests or personal relationships that could have appeared to influence the work reported in this paper.

Data availability

Data will be made available on request.

Acknowledgements

The authors acknowledge Fernando Stanzione for the ICP-MS analyses.

Appendix A. Supplementary material

Supplementary data to this article can be found online at https://doi.org/10.1016/j.seppur.2023.124780.

References

[1] J.C.Y. Jung, P.C. Sui, J. Zhang, A review of recycling spent lithium-ion battery cathode materials using hydrometallurgical treatments, J. Energy Storage. 35 (2021), https://doi.org/10.1016/j.est.2020.102217.
[2] S. Chang, K.H. Young, Y.L. Lien, Reviews of European patents on Nickel/Metal hydride batteries, Batteries. 3 (2017), https://doi.org/10.3390/batteries3030025.
[3] J. Nan, D. Han, M. Yang, M. Cui, Dismantling, recovery, and reuse of spent nickel-metal hydride batteries, J Electrochem Soc. 153 (2006) A101, https://doi.org/10.1149/1.2133721.
[4] W. Linsong, Z. Peng, F. Yu, L. Sujun, Y. Yue, W. Li, S. Wei, Recovery of metals from jarosite of hydrometallurgical nickel production by thermal treatment and leaching, Hydrometall. 198 (2020), https://doi.org/10.1016/j.hydromet.2020.105493.
[5] K.K. Sahu, A. Agarwal, B.D. Pandey, Nickel recovery from spent nickel catalyst, Waste Manag. Res. 23 (2005) 148–154, https://doi.org/10.1177/0734242X05052334.
[6] J. Ramos-Cano, G. González-Zamarripa, F.R. Carrillo-Pedroza, M.D.J. Soria-Aguilar, A. Hurtado-Macías, A. Cano-Vielma, Kinetics and statistical analysis of nickel leaching from spent catalyst in nitric acid solution, Int. J. Miner. Process. 148 (2016) 41–47, https://doi.org/10.1016/j.minpro.2016.01.006.
[7] M. Xiao, D. Han, X. Yang, N. Tsona Tchinda, L. Du, Y. Guo, Y. Wei, X. Yu, M. Ge, Ni-doping-induced oxygen vacancy in Pt-CeO2 catalyst for toluene oxidation: enhanced catalytic activity, water-resistance, and SO2-tolerance, Appl. Catal. B. 323 (2023), 122173, https://doi.org/10.1016/J.APCATB.2022.122173.
[8] M.S.W. Lim, T.C.K. Yang, Y.H. Yap, G.T. Pan, S. Chong, T.J. Tiong, Intensification and optimisation of nickel recovery from spent hydrogenation catalysts via ultrasound-augmented hydrometallurgy, J. Environ. Chem. Eng. 9 (2021), https://doi.org/10.1016/j.jece.2021.105771.
[9] F. Moosakazemi, M.R. Tavakoli Mohammadi, M. Zakeri, M.J. Esmaeili, H. Rafiei, Development of an environmentally friendly flowsheet for the hydrometallurgical recovery of nickel and aluminum from spent methanation catalyst, J. Clean. Prod. 244 (2020). 10.1016/j.jclepro.2019.118731.
[10] P. Johar, C.R. McElroy, E.L. Rylott, A.S. Matharu, J.H. Clark, Biologically bound nickel as a sustainable catalyst for the selective hydrogenation of cinnamaldehyde, Appl. Catal. B. 306 (2022), 121105, https://doi.org/10.1016/J.APCATB.2022.121105.
[11] P.K. Parhi, K.H. Park, G. Senanayake, A kinetic study on hydrochloric acid leaching of nickel from Ni-Al2O3 spent catalyst, J. Ind. Eng. Chem. 19 (2013) 589–594, https://doi.org/10.1016/j.jiec.2012.09.028.
[12] Y. Liu, Q. Song, L. Zhang, Z. Xu, Novel approach of in-situ nickel capture technology to recycle silver and palladium from waste nickel-rich multilayer ceramic capacitors, J. Clean. Prod. 290 (2021), https://doi.org/10.1016/j.jclepro.2020.125650.
[13] Y. Mizuno, T. Hagiwara, H. Chazono, H. Kishi, Effect of milling process on core-shell microstructure and electrical properties for BaTiO3-based Ni-MLCC, J. Eur. Ceram. Soc. 21 (2001) 1649–1652, https://doi.org/10.1016/S0955-2219(01)00084-X.
[14] J.-R. Yoon, M.K. Kim, Electrical characteristics of multilayered ceramic capacitors depending on BaTiO 3 particle size, J. Electr. Eng. Technol. 15 (2020) 2685–2690, https://doi.org/10.1007/s42835-020-00505-7.
[15] H. Kishi, Y. Mizuno, H. Chazono, Base-metal electrode-multilayer ceramic capacitors: past, present and future perspectives, Japan. J. Appl. Phys. Part 1: Regul. Pap. Short Notes Rev. Pap. 42 (2003) 1–5, https://doi.org/10.1143/jjap.42.1.
[16] K. Kaneda, S. Lee, N.J. Donnelly, W. Qu, C.A. Randall, Y. Mizuno, Kinetics of oxygen diffusion into multilayer ceramic capacitors during the re-oxidation process and its implications on dielectric properties, J. Am. Ceram. Soc. 94 (2011) 3934–3940, https://doi.org/10.1111/J.1551-2916.2011.04623.X.

[17] K. Saito, H. Chazono, Stress and electrical field responses of X5R type multilayer ceramic capacitor with Ni internet electrode, Japan. J. Appl. Phys. Part 1: Regul. Pap. Short Notes Rev. Papers. 42 (2003) 6045–6049, https://doi.org/10.1143/jjap.42.6045.
[18] Y. Mizuno, T. Hagiwara, H. Kishi, Microstructural design of dielectrics for Ni-MLCC with ultra-thin active layers, J. Ceram. Soc. Japan (日本セラミックス協会学術論文誌). 115 (2007) 360–364, https://doi.org/10.2109/jcersj.115.360.
[19] K. Hong, T.H. Lee, J.M. Suh, S.H. Yoon, H.W. Jang, Perspectives and challenges in multilayer ceramic capacitors for next generation electronics, J. Mater. Chem. C Mater. 7 (2019) 9782–9802, https://doi.org/10.1039/c9tc02921d.
[20] D. Zhang, Y. Liu, Q. Hu, X. Ke, S. Yuan, S. Liu, X. Ji, J. Hu, Sustainable recovery of nickel, molybdenum, and vanadium from spent hydroprocessing catalysts by an integrated selective route, J Clean Prod. 252 (2020), https://doi.org/10.1016/j.jclepro.2019.119763.
[21] H. Arslanoğlu, A. Yaraş, Recovery of precious metals from spent Mo–Co–Ni/Al2O3 catalyst in organic acid medium: process optimization and kinetic studies, Pet. Sci. Technol. 37 (2019) 2081–2093, https://doi.org/10.1080/10916466.2019.1618867.
[22] F. Odegbemi, G.A. Idowu, A.O. Adebayo, Nickel recovery from spent nickel-metal hydride batteries using LIX-84I-impregnated activated charcoal, Environ. Nanotechnol. Monit. Manag. 15 (2021), https://doi.org/10.1016/j.enmm.2021.100452.
[23] J.-M. Yoo, J.-C. Lee, B.-S. Kim, H.S. Lee, J.-K. Jeong, Leaching of Nickel from a, Hydrodesulphur. Spent Catal. Ammon. Sulfate 37 (9) (2004) 1129–1134, https://doi.org/10.1252/jcej.37.1129.
[24] M.N. Le, M.S. Lee, A review on hydrometallurgical processes for the recovery of valuable metals from spent catalysts and life cycle analysis perspective, Miner. Process. Extr. Metall. Rev. 42 (2021) 335–354, https://doi.org/10.1080/08827508.2020.1726914.
[25] W. Astuti, N.M. Prilitasari, Y. Iskandar, D. Bratakusuma, H.T.B.M. Petrus, Leaching behavior of lanthanum, nickel and iron from spent catalyst using inorganic acids, IOP Conf. Ser.: Mater. Sci. Eng. 285 (2018) 012007.
[26] M.K. Nazemi, F. Rashchi, N. Mostoufi, A new approach for identifying the rate controlling step applied to the leaching of nickel from spent catalyst, Int. J. Miner. Process. 100 (2011) 21–26, https://doi.org/10.1016/j.minpro.2011.04.006.
[27] G. Prabaharan, S.P. Barik, B. Kumar, A hydrometallurgical process for recovering total metal values from waste monolithic ceramic capacitors, Waste Manag. 52 (2016) 302–308, https://doi.org/10.1016/j.wasman.2016.04.010.
[28] E.Y. Yazici, H. Deveci, Cupric chloride leaching (HCl-CuCl2-NaCl) of metals from waste printed circuit boards (WPCBs), Int. J. Miner. Process. 134 (2015) 89–96, https://doi.org/10.1016/j.minpro.2014.10.012.
[29] M. Muscetta, N. Minichino, R. Marotta, R. Andreozzi, I. Di, Zero-valent palladium dissolution using NaCl / CuCl 2 solutions, J. Hazard Mater. 404 (2021), 124184, https://doi.org/10.1016/j.jhazmat.2020.124184.
[30] S. Bhardwaj, D. Dogra, B. Pal, S. Singh, Photodeposition time dependant growth, size and photoactivity of Ag and Cu deposited TiO2 nanocatalyst under solar irradiation, Sol. Energy 194 (2019) 618–627, https://doi.org/10.1016/J.SOLENER.2019.10.055.
[31] E.T. Wahyuni, P.Y. Yulikayani, N.H. Aprilita, Enhancement of visible-light photocatalytic activity of Cu-doped TiO2 for photodegradation of amoxicillin in water, J. Mater. Environ. Sci. 2020 (2020) 670. <http://www.jmaterenvironsci.com> (Accessed July 18, 2023).
[32] Z. Jin, C. Liu, K. Qi, X. Cui, Photo-reduced Cu/CuO nanoclusters on TiO 2 nanotube arrays as highly efficient and reusable catalyst OPEN, 2016. 10.1038/srep39695.
[33] M. Muscetta, R. Andreozzi, R. Marotta, I. Di Somma, Recovery of palladium (II) from aqueous solution through photocatalytic deposition in presence of ZnO under UV/Visible-light radiation, J. Environ. Chem. Eng. 9 (2021), 106523, https://doi.org/10.1016/j.jece.2021.106523.
[34] J. Deng, F. Wu, S. Gao, D.D. Dionysiou, L.Z. Huang, Self-activated Ni(OH)2 cathode for complete electrochemical reduction of trichloroethylene to ethane in low-conductivity groundwater, Appl. Catal. B. 309 (2022), https://doi.org/10.1016/j.apcatb.2022.121258.
[35] H.C. Fu, X.H. Wang, X.H. Chen, Q. Zhang, N.B. Li, H.Q. Luo, Interfacial engineering of Ni(OH)2 on W2C for remarkable alkaline hydrogen production, Appl. Catal. B. 301 (2022), 120818, https://doi.org/10.1016/J.APCATB.2021.120818.
[36] M. Muscetta, L. Clarizia, C. Garlisi, G. Palmisano, R. Marotta, R. Andreozzi, F. Ii, I. Chimica, P. Industriale, Hydrogen production upon UV-light irradiation of Cu / TiO 2 photocatalyst in the presence of alkanol- amines, Int. J. Hydrogen Energy. (2020), https://doi.org/10.1016/j.ijhydene.2020.07.002.
[37] I. Gabriele, F. Bianco, M. Race, S. Papirio, G. Esposito, Phytoremediation of PAH- and Cu-contaminated soil by cannabis sativa L.: preliminary experiments on a laboratory scale, Sustainability (Switzerland) 15 (2023), https://doi.org/10.3390/su15031852.
[38] E.-Y. Kim, J.-C. Lee, B.-S. Kim, M.-S. Kim, J. Jeong, Leaching behavior of nickel from waste multi-layer ceramic capacitors, Hydrometall. 86 (1-2) (2007) 89–95.
[39] G.V.K. Puvvada, R. Sridhar, V.I. Lakshmanan, Chloride Metallurgy: PGM Recovery and Titanium Dioxide Production, JOM 55 (2003) 38–41, https://doi.org/10.1007/s11837-003-0103-1.
[40] P. Vany, Standard Potentials in Aqueous Solutions, Marcel Dekker, 1978.
[41] O. Levenspiel, Chemical Reaction Engineering, 2nd ed., Wiley, 1972.
[42] R. Andreozzi, M. Canterino, V. Caprio, I. Di Somma, R. Sanchirico, Salicylic acid nitration by means of nitric acid/acetic acid system: chemical and kinetic characterization, Org. Process Res. Dev. 10 (2006), https://doi.org/10.1021/op060148o.
[43] H.S. Karapinar, F. Kilicel, F. Ozel, A. Sarilmaz, Fast and effective removal of Pb(II), Cu(II) and Ni(II) ions from aqueous solutions with TiO2 nanofibers: synthesis, adsorption-desorption process and kinetic studies, Int. J. Environ. Anal. Chem. (2021), https://doi.org/10.1080/03067319.2021.1931162.
[44] L. Clarizia, R. Andreozzi, J. Apuzzo, I. Di Somma, R. Marotta, Efficient acetaldehyde production and recovery upon selective Cu/TiO 2-photocatalytic oxidation of ethanol in aqueous solution, Chem. Eng. J. 393 (2020), 123425, https://doi.org/10.1016/j.cej.2019.123425.